# Running Pattern Generation for a Humanoid Robot

Shuuji Kajita (AIST), Takashi Nagasaki (U. of Tsukuba),
Kazuhito Yokoi, Kenji Kaneko and Kazuo Tanie (AIST)
1-1-1 Umezono, Tsukuba Central 2, AIST, Tsukuba Ibaraki 305-8568, Japan
E-mail: s.kajita@aist.go.jp

## Abstract

*A method of running pattern generation for a humanoid robot using the dynamics of a simple inverted pendulum is proposed. Dynamic simulation using a model of an actual humanoid robot shows that the robot can run by applying a generated pattern with slight modifications. The simulation is used to evaluate the required performance of actuators for an actual running robot.*

## 1 Introduction

Research on humanoid robots is currently one of the most exciting topics in the field of robotics and there are many ongoing projects [4, 11, 7, 6, 2]. Most studies focus on biped walking and have already demonstrated reliable dynamic biped walking. Watching those successful demonstrations, we naturally wanted to ask, "Can we build a running humanoid ?"

We believe it is a worthwhile technical challenge for the following reasons. First, study of running will add new functions of mobility to humanoid robots. For example, jumping over large obstacles or a fissure might be achieved using a derivative of running control. Second, studying extreme situations will give us insights into improve the hardware itself. Current robots are too fragile to operate in various environments. We must treat them carefully, even in an experiment of walking at low speed. We expect to overcome this fragility in the process of developing a running humanoid.

Running robots have been intensively studied by Raibert et al.[9] Their famous hopping robots driven by pneumatic and hydraulic actuators performed various actions including somersaults [8]. Using a similar control strategy, Hodgins simulated a running human with computer graphics [5].

Ahmadi and Buehler studied running monopods [1] from the standpoint of energy efficiency. Using a new control strategy, they created an electrically powered running robot that could run at 4.5km/h with a power expenditure of only 48W.

Gienger et al. are also working toward the realization of a biped jogging robot [2]. They have proposed a walking/running controller based on feedback linearization and built a humanoid robot called "Johnnie."
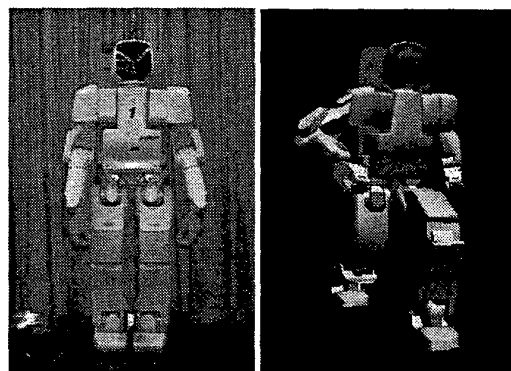


Figure 1: *HRP1 humanoid robot and running simulation*

In this paper, we discuss running as an extended function of the existing *HRP1* humanoid robot (Figure 1). Although actual experiments are not possible, we could simulate running using the actual physical parameters of HRP1.

In Section 2, we introduce a method for running pattern generation using the dynamics of a simple inverted pendulum. Dynamic simulation shows that HRP1 can run using the generated pattern with slight modifications as explained in Section 3. By comparing the actuation results of running and walking, we can estimate the properties required for the actuators of a running humanoid.

## 2 Running pattern for a simple inverted pendulum

In this section, we describe our design of a running pattern for a simple inverted pendulum model.

### 2.1 Dynamics of takeoff

Let us start with a very simple robot that has a point mass of $m$ and a massless telescopic leg (Figure 2). We assume the length of the leg $l$ is controlled as

$$l = l_0 + \alpha \sin \omega t, \qquad (1)$$

where $l_0$, $\alpha$, $\omega$ are the neutral leg length, the amplitude of the vibration and the frequency, respectively.
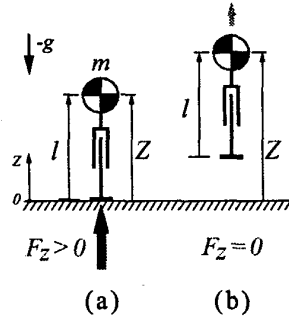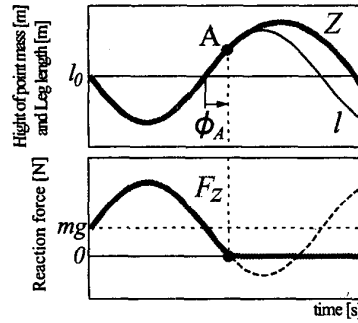


Figure 2: *Take-off model*



Figure 3: *Lift-off sequence*

While the foot is in contact with the ground, the reaction force $F_z$ is given by

$$F_z = m(\ddot{l} + g) = m(-\alpha\omega^2 \sin \omega t + g), \qquad (2)$$

where $g$ is the gravity acceleration. When $\alpha\omega^2 > g$, this equation gives negative $F_z$ in a certain phase (dashed line in Figure 3), but it happens only when the foot is firmly in contact with the ground. Typically, the foot loses contact with the ground as fast as $F_z$ reaches zero and the robot jumps into the air (Figure 2(b), Figure 3). After the robot *takes off* at the point $A$ where the reaction force $F_z$ becomes zero, the robot takes a free fall trajectory. The liftoff timing $\phi_A$ and the speed at the moment of takeoff $\dot{z}_A$ are given by

$$\phi_A = (1/\omega) \sin^{-1}(g/\alpha\omega^2), \qquad (3)$$

and

$$\dot{z}_A = \alpha\omega \cos \omega\phi_A = \sqrt{(\alpha\omega)^2 - (g/\omega)^2}. \qquad (4)$$

### 2.2 Continuous vertical hopping

To design the steady hopping of a biped, we introduce a second model which has two telescopic legs (Figure 4). One half cycle of the hopping motion of this model is illustrated in Figure 5. The bold line curve shows the mass trajectory with a takeoff at point $A$, landing at point $B$ and the second takeoff at point $A'$. The right leg motion $l_R$ is shown by the dashed line $S$-$A$-$C$-$C'$-$B'$ and the left leg motion $l_L$ by the thin line $D$-$B$-$A'$-$D'$.
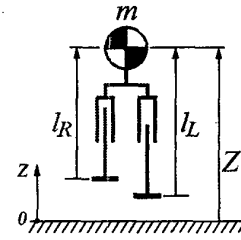


Figure 4: *Biped model*

To have a takeoff at point $A$, the right leg is driven from point $S$ to $C$ by

$$l_R = l_0 + \alpha \sin \omega t. \qquad (5)$$

For the landing point, we specify point $B$ to be the same height as point $A$. From this condition, the duration of the flight phase $T_{flight}$ is calculated as

$$T_{flight} = 2\dot{z}_A/g. \qquad (6)$$

To achieve a smooth landing, we determine the motion of the left leg $D$-$B$-$A'$-$D'$ as

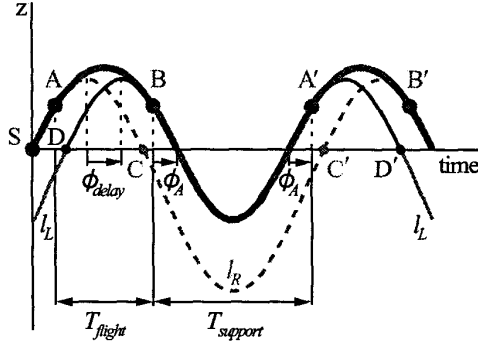$$l_L = l_0 + \alpha \sin \omega(t - \phi_{delay}), \qquad (7)$$

Figure 5: *Continuous hopping motion*

$$\phi_{delay} \equiv T_{flight} - 2(\frac{\pi}{2\omega} - \phi_A). \tag{8}$$

In this pattern, the velocity and acceleration of the mass change continuously at the moment of landing. From point $B$, the robot is supported by the left leg and has a take off at point $A'$. The duration of the support phase is given by

$$T_{support} = (\pi/\omega) + 2\phi_A. \tag{9}$$

To have a landing at point $B'$, we give the right leg trajectory from point $C'$ to $B'$ as

$$l_R = l_0 + \alpha \sin \omega(t - 2\phi_{delay}). \tag{10}$$

During left leg support, the right leg must be in the air. For this purpose, the curve between point $C$ and $C'$ is interpolated to avoid collision with the floor.

With the given parameters $\alpha$ and $\omega$, we can easily calculate the flight and support times $(T_{flight}, T_{support})$ using Eqs. (3),(4),(6) and (9). To obtain $\alpha$ and $\omega$ for the specified $T_{flight}$ and $T_{support}$, we used Newton's method with these equations.

## 2.3 Sagittal and lateral motion generation

The design of the horizontal element of running is also based on inverted pendulum dynamics. Figure 6 illustrates the inverted pendulum in the sagittal ($x$-$z$) plane. For an ideal condition, we assume the torque around the contact point equals zero ($\tau_y = 0$) . This results the constraint between floor reaction forces and mass location as

$$\frac{F_x}{F_z} = \frac{x}{z}, \tag{11}$$

where $F_x$ and $x$ are the horizontal floor reaction force and the horizontal position, respectively.
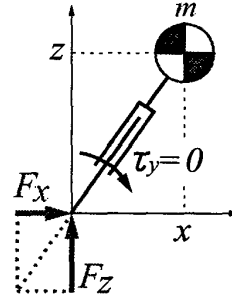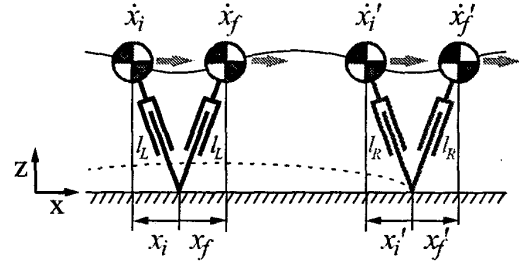


Figure 6: *Horizontal balance*



Figure 7: *Horizontal motion*

When the vertical element is given by Eqs.(1) and (2), we can calculate the horizontal dynamics as follows,

$$\ddot{x} = \frac{1}{m}F_x \tag{12}$$

$$= \frac{-\alpha\omega^2 \sin \omega t + g}{l_0 + \alpha \sin \omega t}x. \tag{13}$$

Note that this is the equation for the support phase where $\frac{\pi}{\omega} - \phi_A < t < \frac{2\pi}{\omega} + \phi_A$.

Figure 7 shows two successive support phases with a flight phase between them. Since Eq.(13) is deterministic with a given initial condition, we modify the horizontal touchdown position $x_i$ to control the running speed. For this purpose, we used Raibert's feedback law [9],

$$x_i' = -\frac{\dot{x}_f T_{support}}{2} - k_{\dot{x}}(\dot{x}_f - \dot{x}_d), \tag{14}$$

where $\dot{x}_d$ is the desired running speed and $k_{\dot{x}}$ is the feedback gain.

The feedback gain $k_{\dot{x}}$ is calculated as follows. By integrating Eq.(13), we have the relationship between the initial condition $(x_i, \dot{x}_i)$ and the final condition $(x_f, \dot{x}_f)$ for each support phase as follows,

$$x_f = \Phi(x_i, \dot{x}_i, T_{support}), \tag{15}$$

$$\dot{x}_f = \dot{\Phi}(x_i, \dot{x}_i, T_{support}). \qquad (16)$$

Although we cannot obtain the analytical form of the functions $\Phi$ and $\dot{\Phi}$, we have the linear relationship of the small deviation from the target running pattern as

$$\begin{pmatrix} \Delta x_f \\ \Delta \dot{x}_f \end{pmatrix} = J_\Phi \begin{pmatrix} \Delta x_i \\ \Delta \dot{x}_i \end{pmatrix}, \qquad (17)$$

where

$$J_\Phi \equiv \begin{pmatrix} \Delta\Phi/\Delta x_i & \Delta\Phi/\Delta \dot{x}_i \\ \Delta\dot{\Phi}/\Delta x_i & \Delta\dot{\Phi}/\Delta \dot{x}_i \end{pmatrix}, \qquad (18)$$

which is numerically calculated around an ideal running pattern.

The relationship between the final condition and the next initial condition is explained as

$$\begin{pmatrix} \Delta x_i' \\ \Delta \dot{x}_i' \end{pmatrix} = K \begin{pmatrix} \Delta x_f \\ \Delta \dot{x}_f \end{pmatrix}, \qquad (19)$$

where

$$K \equiv \begin{pmatrix} 0 & -T_{support}/2 - k_{\dot{x}} \\ 0 & 1 \end{pmatrix}. \qquad (20)$$

This represents the control law of Eq.(14) and horizontal speed conservation in the flight phase.

By combining Eqs.(17) and (19), the transition from step to step is given as

$$\begin{pmatrix} \Delta x_i' \\ \Delta \dot{x}_i' \end{pmatrix} = K J_\Phi \begin{pmatrix} \Delta x_i \\ \Delta \dot{x}_i \end{pmatrix}. \qquad (21)$$

From the stable condition of the digital controller, the running system should satisfy

$$|\lambda| < 1, \quad \det(\lambda I - K J_\Phi) = 0. \qquad (22)$$

Therefore, feedback gain $k_{\dot{x}}$ is calculated from this equation.

For lateral($y$-$z$) motion generation, we adopted the same method.

# 3 Running simulation of a humanoid robot

## 3.1 Model and simulator

We evaluated our running pattern in a computer simulation using the physical parameters of the HRP1 existing humanoid robot (Figure 1). HRP1 is a platform developed in an R&D project of the Ministry of Economy, Trade and Industry (METI) of Japan [6]. Its dimensions are 1600 [mm] height, 600 [mm] width, and 117 [kg] weight with batteries, and the robot has 12 d.o.f. in two legs and 16 d.o.f. in two arms including hands with 1 d.o.f. grippers.

For the dynamic simulation, we used the *OpenHRP* simulator which was also developed in the same project [3]. The robot data is given in an extended VRML format which combines the dynamic parameters and the geometric shapes of the links. We also modeled the effect of the rotor inertia of the servomotors.

In our simulation, we assumed the center of mass of the total robot to be at a fixed point on the robot body. With this approximation, the body motion corresponds to the inverted pendulum of Figure 7. The joint angles and angular velocities were calculated by inverse kinematics and served as the reference for PD feedback control,

$$\tau = k_p(\theta_d - \theta) + k_v(\dot{\theta}_d - \dot{\theta}), \qquad (23)$$

where $(\theta_d, \dot{\theta}_d)$ is the reference joint state calculated by inverse kinematics, $(\theta, \dot{\theta})$ is the actual state and $(k_p, k_v)$ is the set of feedback gains.

## 3.2 Modification of running pattern

We designed a running pattern of 3.3m/s (11.9km/h) using our proposed method. The detailed parameters are shown in Table 1.

Table 1: *Simulated running pattern*

| $\dot{x}_d$ | 3.3 m/s | $l_0$ | 0.521 m |
|---|---|---|---|
| $T_{support}$ | 0.18 s | $\omega$ | 24.2 rad/s |
| $T_{flight}$ | 0.12 s | $\alpha$ | 0.0296 m |
| | | $k_{\dot{x}}$ | 0.24 m/(m/s) |

In the first simulation, we observed that the robot kicked the floor twice for each half-cycle. As a result, the robot fell down as fast as it started running. Figure 8 shows the vertical height and leg length at zero running speed. This problem arose because the original hopping pattern was designed for a concentrated single point mass model while the target model has multibody dynamics. As such, the robot did not get enough upward momentum and touched down earlier than expected. Since the foot collided with the floor too fast at the first touchdown, the robot had a small rebound before the second touchdown.

To achieve the expected landing, the vertical leg trajectory just before the landing time was modified relative to the flight trajectory of the robot body (Figure 9). After the landing, the motion resumes its original trajectory to achieve the next takeoff. The original
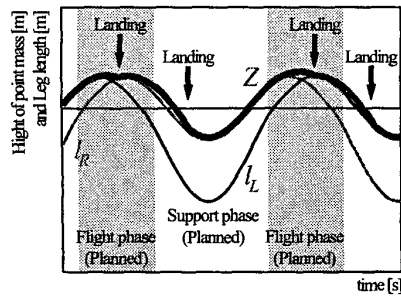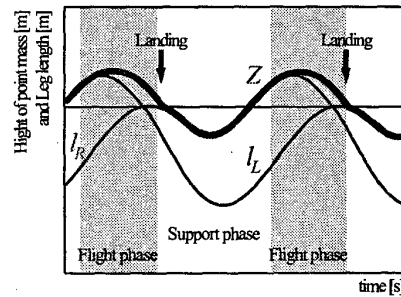
Figure 8: *Unexpected touchdown*



Figure 9: *Modified trajectory*

horizontal element of the leg trajectory was retained. With this modification, we could simulate a running motion from zero speed to the target speed. However, when the target speed was high (> 0.3 m/s), the running direction unexpectedly changed because of the yaw moment generated by leg swing. To compensate for this effect, we introduced arm swing by

$$x_{wrist} = k_{arm} x_{foot}, \qquad (24)$$

where $x_{foot}$ is the horizontal displacement of the foot and $x_{wrist}$ is the horizontal displacement of the wrist on the same side. All of these variables are measured along the running direction relative to the waist. Since we chose to set parameter $k_{arm}$ as $-0.6$, this rule makes the robot arm swing in the opposite direction from the leg swing and yields proper yaw moment compensation. With this modification, the simulated robot could run straight at the specified target speed of 3.3m/s. Figure 10 shows the running speed of the planned pattern and the speed of the humanoid robot. The running speed (2.9m/s) slower than the reference (3.3m/s) was caused by the robot feet slipping on the floor. Figure 11 shows snapshots of the simulation.
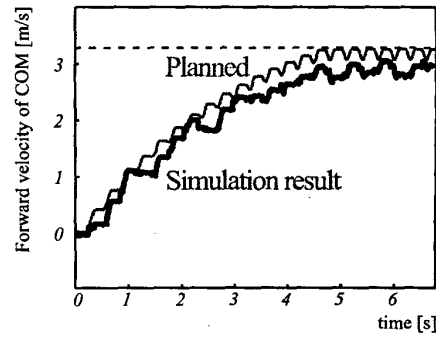


Figure 10: *Running speed of the simulation*

### 3.3 Joint drive requirements

As the joints which have the most important role in running, we focus on the crotch pitch joints, the knee joints and the ankle pitch joints. Figure 12, 13 and 14 show the angular velocities, torques and power of those joints respectively in the simulation shown in Figure 10 and 11. In each graph, the thin line indicates the right leg data and the bold line indicates the left leg data. The vertical dotted lines indicate the timing of phase transition. The running phase is displayed at the top of the crotch graph. The horizontal dotted line, the horizontal thin line and the horizontal bold line are the flight phase, support phase of the right leg, and support phase of the left leg, respectively.

An interesting result is that the peak power occurs in the flight phase. This is prominent in the knee joint (shown by arrows in Figure 14). This reminds us of Ahmadi and Buehler's remark that a large part of a running monopod's power is consumed in the flight phase [1].
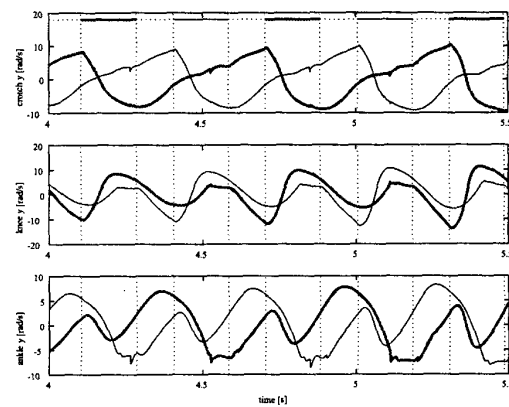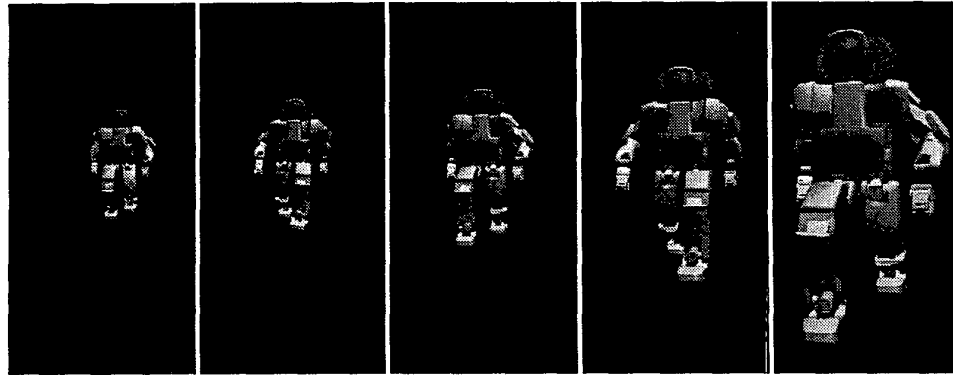


Figure 12: *Joint speed*

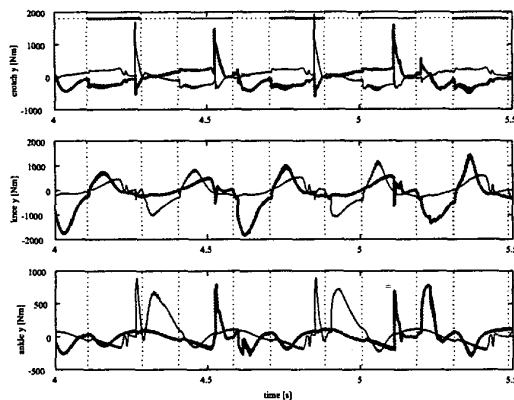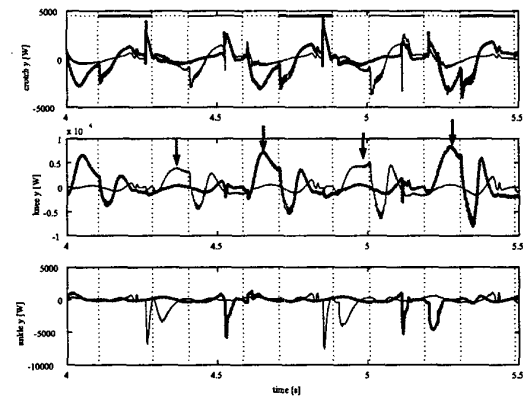Figure 11: *Snapshots of running simulation*



Figure 13: *Joint torque*



Figure 14: *Joint power*

Table 2 shows the maximum value of the absolute data in the Figure 12, 13 and 14. It also shows the average of the absolute powers. The parenthesized figures in the table indicate the ratio to the corresponding data for walking at 0.5 [m/s] shown in Table 3. The increasing ratio of the joint speeds (2.4 – 3.7) is considered small for a moving speed that is about six times faster. This is understandable because a large part of running transportation is done in the flight phases. Instead, the increasing ratio of the joint torques are between 7.3 and 9.2 compared to those in walking. The increasing ratio of the peak joint powers are between 28 and 56. Apparently, though our HRP1 humanoid robot does not meet these requirements, we clearly need actuators that are at least 28 to 56 times more powerful for our running pattern.

Table 4 shows the comparison between the robot and a human running with 2.72m/s[10]. We observe our robot consumes power which is about ten times bigger than the human runner. It suggests that the robot could run more efficiently by improving our running pattern.

## 4    Conclusions

This paper introduced a method of running pattern generation. Although it is based on a simple inverted pendulum model, a model of an actual humanoid robot could run successfully in the dynamic simulator by applying a small modification. Using the results of simulation, we estimated the required power specification for a running humanoid.

To build an actual running robot, we still need to investigate pattern generation and power analysis. Finding an energy-efficient running pattern will be our next target.

Table 2: *Actuator requirement for running at 2.9m/s*

| speed [rad/s] | crotch | knee | ankle |
|---|---|---|---|
| *peak of abs.* | 10.4 (3.1)† | 13.6 (3.7) | 8.63 (2.4) |
| torque [Nm] | crotch | knee | ankle |
| *peak of abs.* | 1940 (9.2) | 1830 (7.3) | 897 (7.9) |
| power [W] | crotch | knee | ankle |
| *peak of abs.* | 4570 (30) | 8480 (28) | 7530 (56) |
| *average of abs.* | 798 (27) | 1590 (19) | 447 (15) |

† Parenthesized numbers indicate the increasing ratio from walking at 0.5 [m/s] shown in Table 3.

Table 3: *Actuator requirement for walking at 0.5m/s*

| speed [rad/s] | crotch | knee | ankle |
|---|---|---|---|
| *peak of abs.* | 3.37 | 3.71 | 3.59 |
| torque [Nm] | crotch | knee | ankle |
| *peak of abs.* | 211 | 249 | 113 |
| power [W] | crotch | knee | ankle |
| *peak of abs.* | 151 | 301 | 135 |
| *average of abs.* | 30.1 | 82.5 | 29.9 |

Table 4: *Peak power normalized by weight, robot and human runner*

| normalized power [W/kg] | crotch | knee | ankle |
|---|---|---|---|
| *HRP1* | 38.9 | 72.2 | 64.1 |
| *Human†* | 3.2 | 6.9 | 8.7 |

†weight 79kg, running speed =2.72m/s[10].

# References

[1] Ahmadi, M. and Buehler, M., "The ARL Monopod II Running Robot: Control and Energetics", Proc. of the 1999 ICRA, pp.1689–1694, 1999.

[2] Gienger, M., et.al, "Toward the Design of a Biped Jogging Robot," Proc. of the 2001 ICRA, pp.4140–4145, 2001.

[3] Hirukawa, H., Kanehiro, F., Kajita, S., "OpenHRP: Open Architecture Humanoid Robotics Platform," Intr. Symposium on Robotics Research (ISRR), Melbourne, November 2001 (printing).

[4] Hirai, K., Hirose, M., Haikawa, Y. and Takenaka, T., "The Development of Honda Humanoid Robot," Proc. of the 1998 ICRA, pp.1321–1326, 1998.

[5] Hodgins, J.K., "Three-Dimensional Human Running," Proc. of the 1996 ICRA, pp.3271–3277, 1996.

[6] Inoue, H., Tachi, S., Nakamura, Y., Hirai, K., et.al, "Overview of Humanoid Robotics Project Of METI," Proc. Int. Symp. Robotics, pp.1478–1482, 2001.

[7] Nishiwaki, K., Sugihara, T., Kagami, S., Kanehiro, F., Inaba, M., and Inoue, H., "Design and Development of Research Platform for Perception-Action Integration in Humanoid Robot: H6," Proc. Int. Conference on Intelligent Robots and Systems, pp.1559–1564, 2000.

[8] Playter, Robert R. and Raibert, Marc H., "Control of a Biped Somersault in 3D," Proc. of IFToMM-jc International Symposium on Theory of Machines and Mechanisms (in Nagoya, Japan), pp.669–674, 1992.

[9] Raibert, M., *Legged Robots that Balance*, Cambridge, MA, MIT Press, 1986.

[10] Winter, D., "Moments of Force and Mechanical Power in Jogging," J. of Biomechanics, vol.16, no.1, pp.91–97, 1983.

[11] Yamaguchi, J., Soga, E., Inoue, S. and Takanishi, A., "Development of a Bipedal Humanoid Robot – Control Method of Whole Body Cooperative Dynamic Biped Walking –," Proc. of the 1999 ICRA, pp.368–374, 1999.